Numerical simulation of magnons

Sondre Duna Lundemo†
Department of Physics, Norwegian University of Science and Technology, Trondheim
Norway
TFY4235 - Computational physics
(*Last updated on March 8, 2021*)

†sondre@duna.no

Contents

PART I

Introduction

1 Theoretical background

The hamiltonian governing the dynamics of a chain of spins is

$$H = -\frac{1}{2}\sum_{j,k}^{N} J_{jk}\mathbf{S}_j \cdot \mathbf{S}_k - d_z \sum_{j=1}^{N}(S_{j,z})^2 - \mu \sum_{j=1}^{N} \mathbf{B}_j \cdot \mathbf{S}_j, \tag{1}$$

And the time-dependence is governed by the Landau-Lifshitz-Gilbert equation (LLG)

$$\frac{\mathrm{d}\mathbf{S}_j}{\mathrm{d}t} = \frac{-\gamma}{\mu(1+\alpha^2)}\left[\mathbf{S}_j \times \mathbf{H}_j + \alpha \mathbf{S}_j \times (\mathbf{S}_j \times \mathbf{H}_j)\right] \tag{2}$$

where

$$\mathbf{H}_j = -\frac{\partial H}{\partial \mathbf{S}_j} + \boldsymbol{\xi}_j. \tag{3}$$

In the absence of noise, $\boldsymbol{\xi}_j \equiv 0$, we can find an explicit relation for the effective field $\mathbf{H}_j$ in (3). This can be done by noting that

$$\begin{aligned}
-\frac{\partial H}{\partial \mathbf{S}_j} &= \frac{1}{2}\sum_{i,k}^{N} J_{ik}\frac{\partial}{\partial \mathbf{S}_j}(\mathbf{S}_i \cdot \mathbf{S}_k) + d_z \sum_{i=1}^{N}\frac{\partial}{\partial \mathbf{S}_j}(\mathbf{S}_i \cdot \mathbf{e}_z)^2 + \mu \sum_{i=1}^{N}\frac{\partial}{\partial \mathbf{S}_j}\mathbf{B}_i \cdot \mathbf{S}_i \\
&= \frac{1}{2}\sum_{i,k}^{N} J_{ik}\left(\delta_{ij}\mathbf{S}_k + \delta_{jk}\mathbf{S}_i\right) + d_z \sum_{i=1}^{N} 2\delta_{ij}(\mathbf{S}_i \cdot \mathbf{e}_z)\mathbf{e}_z + \mu \sum_{i=1}^{N}\mathbf{B}_i\delta_{ij} \\
&= \sum_{i=1}^{N} J_{ij}\mathbf{S}_i + 2d_z S_{j,z}\mathbf{e}_z + \mu\mathbf{B} \\
&= \sum_{i\in\mathcal{N}_j} J_{ij}\mathbf{S}_i + 2d_z S_{j,z}\mathbf{e}_z + \mu\mathbf{B},
\end{aligned}$$

where we in the last transition have made further simplifications by only performing the sum over the nearest neighbours $\mathcal{N}_j$ of j. Using this expression we might rewrite the LLG in (2) as

$$\begin{aligned}
\frac{\mathrm{d}\mathbf{S}_j}{\mathrm{d}t} = \frac{-\gamma}{\mu(1+\alpha^2)}\Bigg[&\mathbf{S}_j \times \left(\sum_{i\in\mathcal{N}_j} J_{ij}\mathbf{S}_i + 2d_z S_{j,z}\mathbf{e}_z + \mu\mathbf{B}\right) \\
&+\alpha\mathbf{S}_j \times \left[\mathbf{S}_j \times \left(\sum_{i\in\mathcal{N}_j} J_{ij}\mathbf{S}_i + 2d_z S_{j,z}\mathbf{e}_z + \mu\mathbf{B}\right)\right]\Bigg].
\end{aligned}$$

PART
II

Code overview

2 General structure

3 Remarks on performance

PART III

Results and discussion

4 Single spin

4.1 Precession of spin in uniform magnetic field

We simulate the time evolution of a single spin $\mathbf{S}$ in the presence of a uniform magnetic field $\mathbf{B} = (0, 0, B_0)^T$ in the $\mathbf{e}_z$-direction. The components of the spin at equidistant time steps during one period are shown in figure 1. As expected, we see that the spin precesses around the effective field $\mathbf{H}$, which in this case is given by

$$\mathbf{H} = -\frac{\partial H}{\partial \mathbf{S}} = \frac{\partial}{\partial \mathbf{S}} (\mu \mathbf{B} \cdot \mathbf{S}) = \mu \mathbf{B},$$

in the absence of damping and anisotropy.

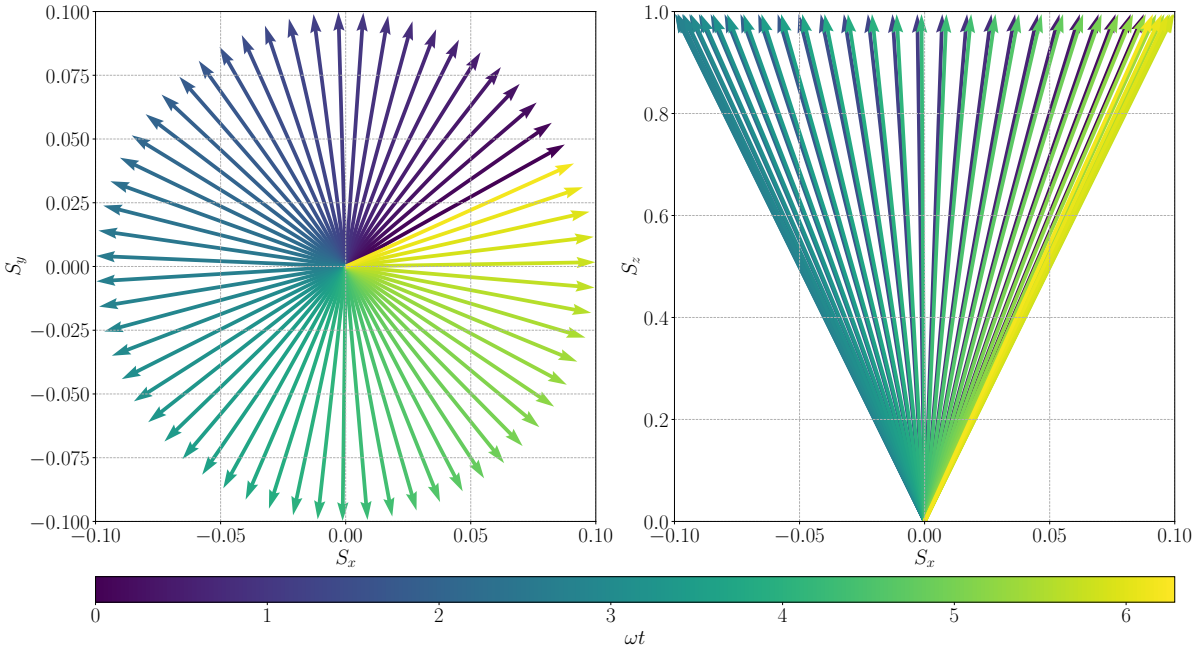

Figure 1: The figure shows the x and y component of the spin during one period in a uniform magnetic field without further interactions.

In this particular case, we can easily find an analytical solution to compare with. The LLG-equation reads

$$\partial_t \mathbf{S} = -\gamma \mathbf{S} \times \mathbf{B}.$$

As $\mathbf{B} = (0, 0, B_0)^T$,

$$\mathbf{S} \times \mathbf{B} = (S_y \mathbf{e}_x - S_x \mathbf{e}_y) B_0.$$

Thus, we have two equations

$$\begin{cases} \partial_t S_x = -\gamma B_0 S_y \\ \partial_t S_y = \gamma B_0 S_x. \end{cases} \tag{4}$$

which are easily solved by differentiating both with respect to t, and then substituting the first order derivatives on the right hand side by the corresponding expressions in 4.

$$\begin{cases} \partial_t^2 S_x = -\gamma B_0 \partial_t S_y \\ \partial_t^2 S_y = \gamma B_0 \partial_t S_x. \end{cases} \tag{5}$$

This yields the two equations

$$\ddot{S}_x = -\left(\gamma B_0\right)^2 S_x \quad ; \quad \ddot{S}_y = -\left(\gamma B_0\right)^2 S_y, \tag{6}$$

which have solutions

$$S_x(t) = S_x(0)\cos\left(\omega t\right) - S_y(0)\sin\left(\omega t\right) \tag{7}$$
$$S_y(t) = S_y(0)\cos\left(\omega t\right) + S_x(0)\sin\left(\omega t\right), \tag{8}$$

with the frequency $\omega = \gamma B_0$. When comparing the exact solution with the numerical estimate obtained through integrating the LLG-equation with Heun's method, the trajectories of S_x and S_y are as shown in figure 2.

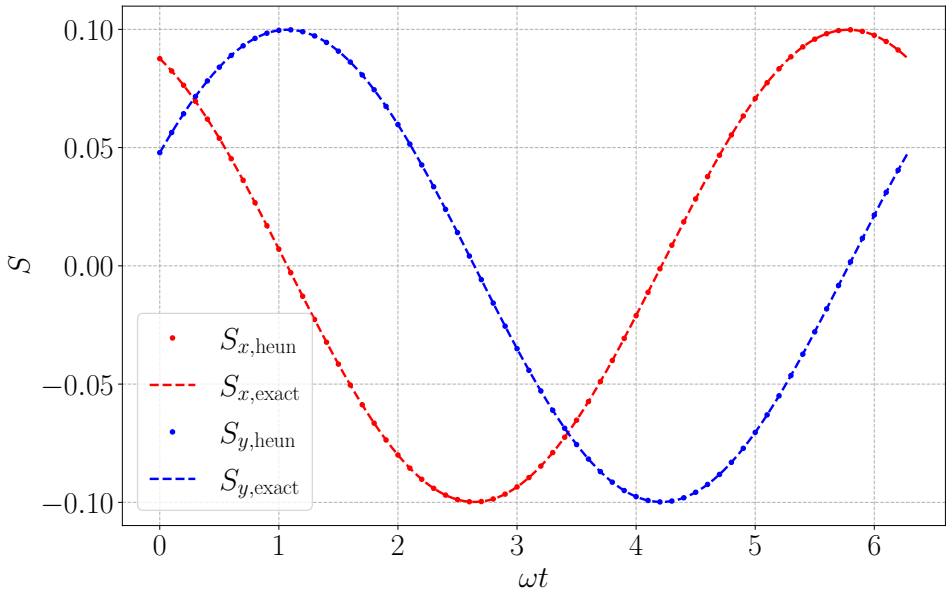

Figure 2: The plot shows the exact solution given in (7) and (8) compared with the numerical solution sampled at every tenth step to be able to distinguish the paths.

It is perhaps more enlightening to consider the pointwise difference of the exact and numerical solution. This is shown in figure 3. The figure shows that the deviations locally oscillate, and that the absolute global deviations increase with time as we'd expect. Further considerations on the deviations are considered in 4.2.

4.2 Error analysis

For the error analysis, I choose 10 logarithmically spaced step-lengths from 10^{-5} to 10^{-1}. As a measure of the *global error*, that is the cumulated error over one period. The error as a function of step length is shown in figure 4.

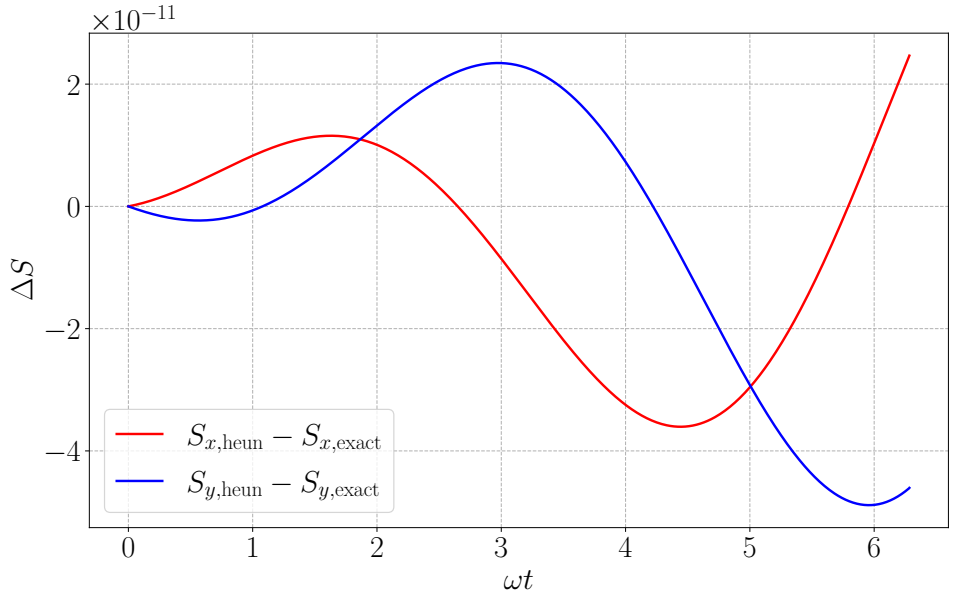

Figure 3: The plot shows the difference between the exact solutions given in (7) and (8), and the numerical solutions over one period.

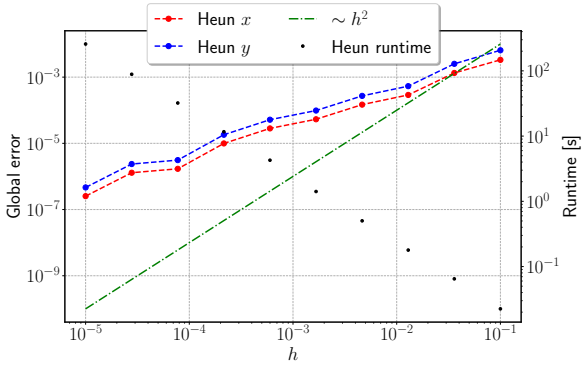

Figure 4: Error as a function of step length for Heun's method.

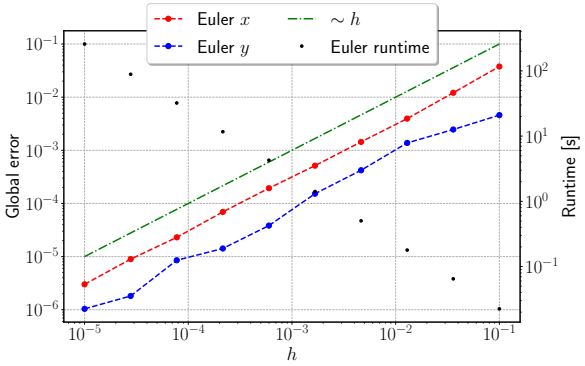

Figure 5: Error as a function of step length for Euler's method.

Since Heun's method is of second order, we would expect its slope in a log-log plot to be roughly 2. However, as demonstrated in figure 4, the slope is slightly less than 2. This is due to FIND REASON FOR THIS. In figure 5 we have plotted the errors for Euler's method for the same step lengths. This plot clearly demonstrates the well known fact that Euler's method is of order 1.

4.3 Damped precession of spin in magnetic field

Next, we include damping in the model. This amounts to setting $\alpha \neq 0$. The plots of the trajectories in the x and y direction for three different damped cases is shown in figure 6. The damping lifetime $\tau = \frac{1}{\alpha\omega}$ is fitted to the plots by plotting

$$\pm\sqrt{S_x^2 + S_y^2}\exp\left(-\alpha\omega t\right),$$

which is approximately the shape of the envelope in the presence of damping.

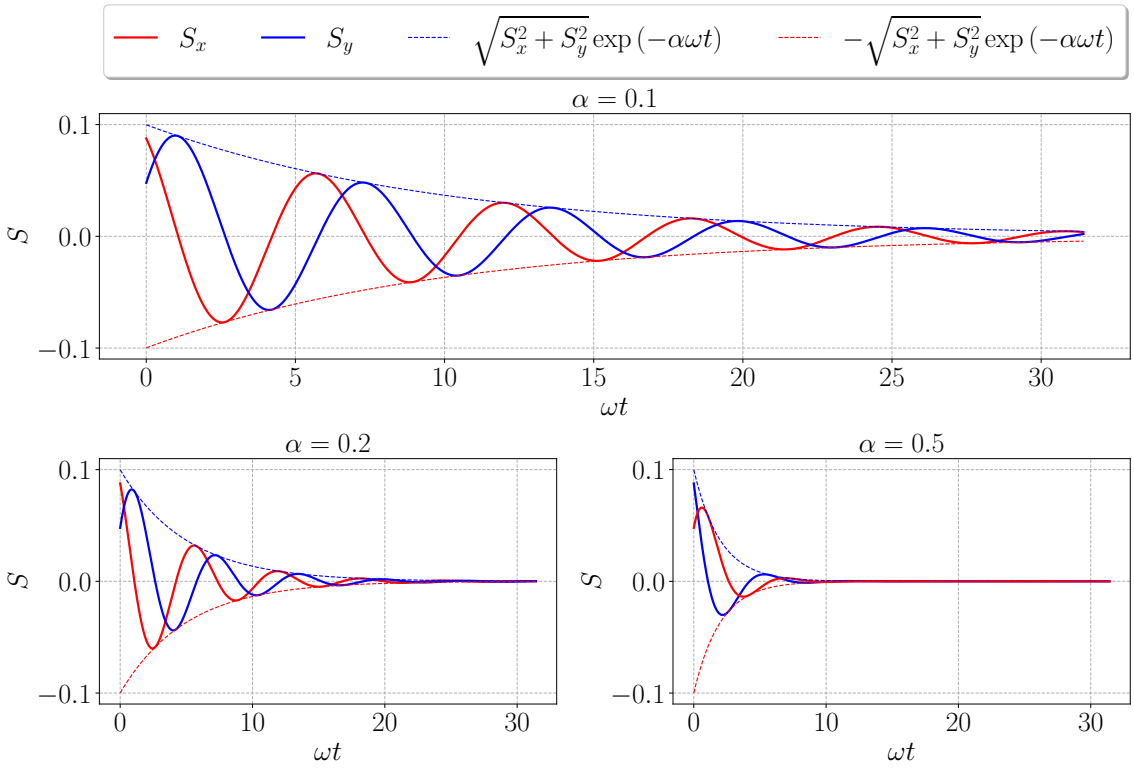

Figure 6: Three different damped precessions.

5 The spin chain

5.1 Ground states

In this section we initialise 10 spins in random directions and simulate the time evolution for $J < 0$ and $J > 0$. The plots of the z-component of each of the spins over time is shown in figure 7 and 8. What is evident from these plots is that a positive coupling constant J tends to make the spins align with their neighbours, while the negative constant tends to make them oppose them. This is a fact that is readily seen from inspecting the hamiltonian in (1), since a positive J makes the maximum of $\sum_{j,k} \mathbf{S}_j \cdot \mathbf{S}_k$ most energetically favourable, while a negative one makes its minimum most favourable. These two cases correspond to a ferromagnetic and anti-ferromagnetic system respectively.

The reason for this being apparent when only plotting the S_z-component is the non-zero anisotropy-constant d_z. As seen from the hamiltonian, setting this positive will favour spins in the z-direction. This is also the reason that approximately half of the spins in the case of $J < 0$ being directed along $\mathbf{e}_z$ while the others are directed along $-\mathbf{e}_z$.

5.2 The magnon

5.2.1 Uncoupled system

We initialise the system of 10 spins with random orientations in space and set $J = 0$, $d_z = 1$, $\alpha = 0$ to demonstrate that all the spins precess in time. The trajectories of the

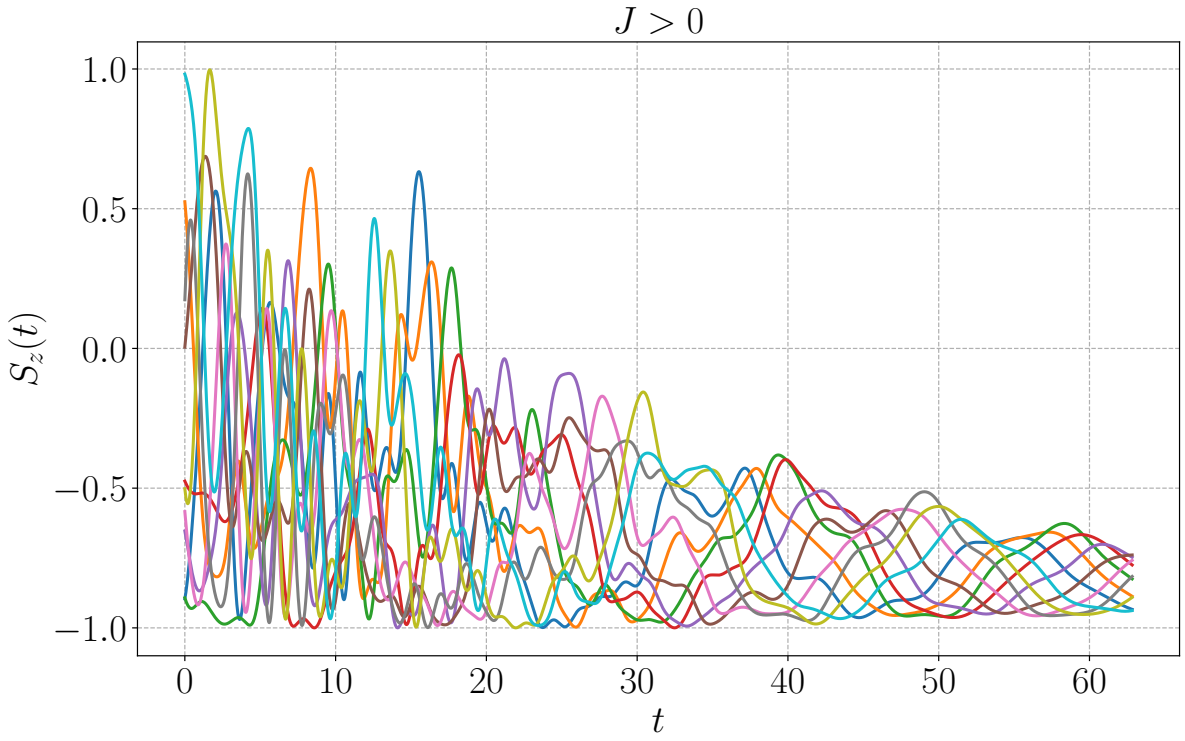

Figure 7: The figure shows the plot of the z-component of the spin of 10 spins in a system of positive coupling constant $J > 0$.

x and y components of the spins is plotted in figure 9

Next, we initialise all the spins along the z direction except for one of them which we tilt slightly. Since there is no coupling between the spins, the precession of the first spin will not affect the others. Furthermore, when $\mathbf{S} = S\mathbf{e}_z$, the right hand side of the LLG (2) will be zero since the effective field is $\| \mathbf{e}_z$. As expected, this is also what is observed when simulating the system. This is shown in figure 10.

5.2.2 Coupled system

If we repeat the procedure used in the previous section except that we couple the spins with $J > 0$, we will observe that all the spins will start to precess, even if they are initialised along the z-axis. This is shown in figure 11. Since the time evolution is hard to catch on a 2d plot I have made a video showing the same as figure 11 here. What is apparent here is that the neighbouring spins couple to each other. Since we are dealing with a finite system, I have chosen to use periodic boundary conditions, so that the first spin affects the last one and vice versa. Implementing this in python requires no effort at all as we can access the left hand neighbour of spin `i` with `i-1` regardless of the value of `i`, and the right hand neighbour with `(i-1)%n` where `n` is the number of spins. This looks a bit artificial in the video, but it corresponds physically to arranging the linear chain in a circle. Another choice of boundary conditions is to simply say that the first and last spin only has *one* neighbour.

If we are to simulate an infinite system we obviously cannot use a discrete model. How-

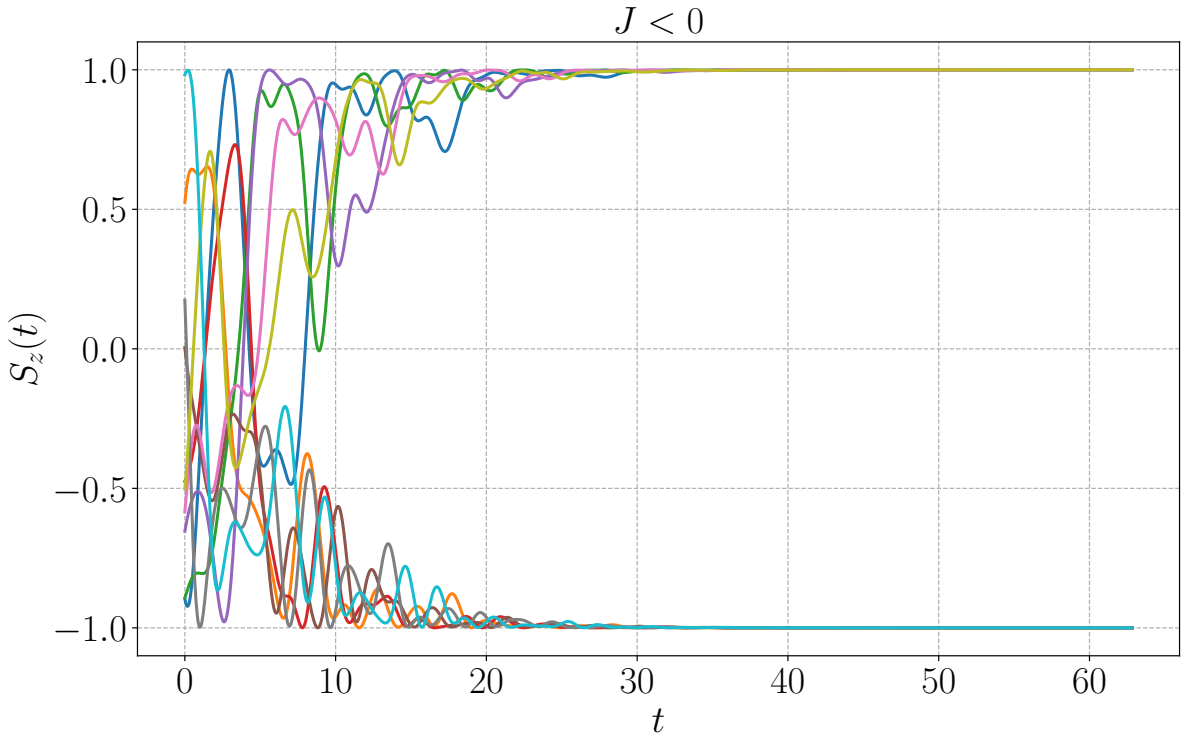

Figure 8: The figure shows the plot of the z-component of the spin of 10 spins in a system of negative coupling constant $J < 0$.

ever, the simulations above suggests that in the limit of *many* spins we can describe the chain as a continuous wave. Then we would have to associate to every index j a position in space

$$\mathbf{S}_j(t) \to \mathbf{S}(\mathbf{x}, t) \quad ; \quad j \to \mathbf{x},$$

where $\mathbf{x}$ is the position of spin j. If we approximate the directional derivatives along a lattice vector $\mathbf{a}$ by the finite differences

$$\|\mathbf{a}\|^2 \nabla^2 \mathbf{S}(\mathbf{x}, t) \approx \|\mathbf{a}\|^2 \frac{\mathbf{S}(\mathbf{x} - \mathbf{a}, t) - 2\mathbf{S}(\mathbf{x}, t) + \mathbf{S}(\mathbf{x} + \mathbf{a}, t)}{\|\mathbf{a}\|^2}$$

and

$$\mathbf{a} \cdot \boldsymbol{\nabla} \mathbf{S}(\mathbf{x}, t) \approx \|\mathbf{a}\| \frac{\mathbf{S}(\mathbf{x} + \mathbf{a}, t) - \mathbf{S}(\mathbf{x} - \mathbf{a}, t)}{2\|\mathbf{a}\|},$$

we see that

$$\mathbf{S}_{j-1}(t) + \mathbf{S}_{j+1}(t) \to \mathbf{S}(\mathbf{x}, t) + \mathbf{a} \cdot \boldsymbol{\nabla} \mathbf{S}(\mathbf{x}, t) + \frac{\|\mathbf{a}\|^2}{2} \nabla^2 \mathbf{S}(\mathbf{x}, t) + \mathcal{O}(\|\mathbf{a}\|^2).$$

Hence, in the limit of small lattice spacings $\|\mathbf{a}\| \to 0$ it should be possible to recast the LLG equation in a continuous form, as a PDE rather than an ode. A self contained discussion of this can be found in [1].

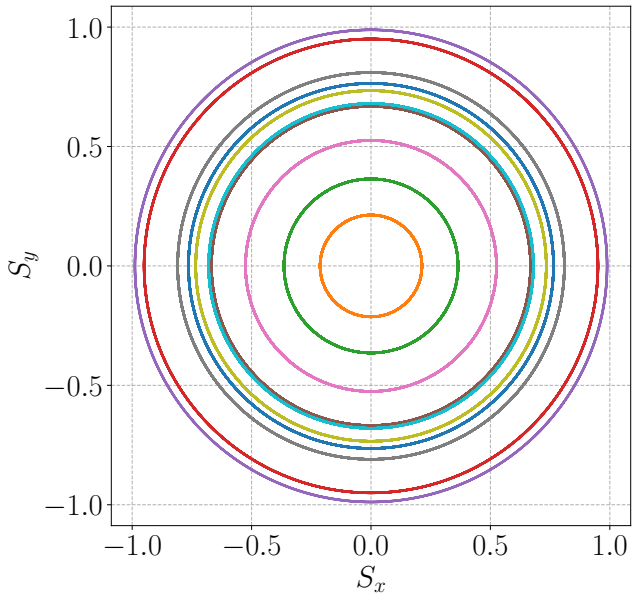

Figure 9: Trajectories of the x and y components of the 10 randomly initialised spins.

PART
IV

Conclusion

References

[1] M. Lakshmanan. The fascinating world of the Landau-Lifshitz-Gilbert equation: An overview, mar 2011.

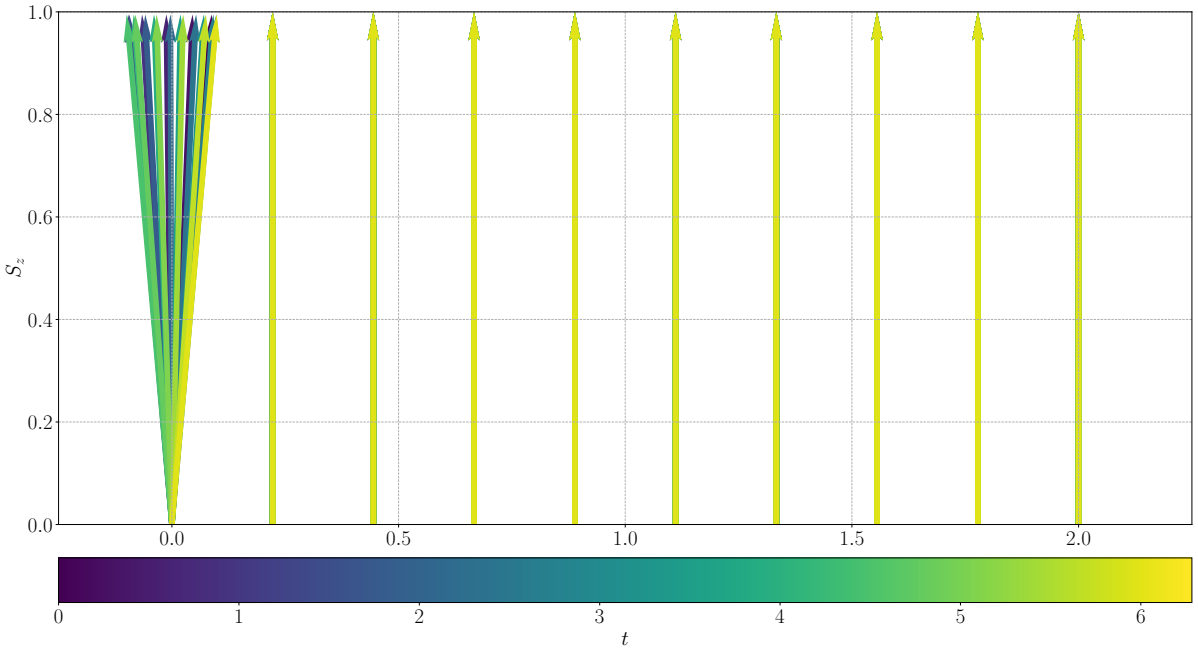

Figure 10: The figure shows uncoupled oscillations of the spin chain.

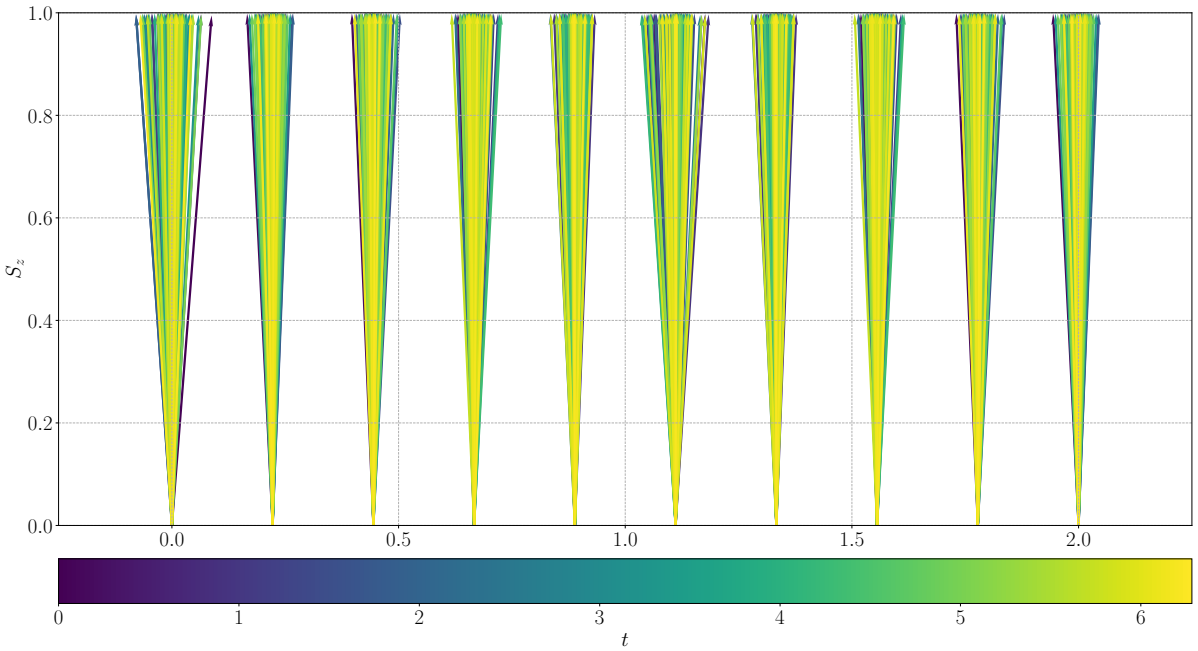

Figure 11: The figure shows coupled oscillations of the spins. A video displaying the same data set can be found here.